Shock Immunity Enhancement via Resonance Damping in Gyroscopes for Automotive Applications

E. Marchetti, L. Fanucci
Dept. of Information Engineering, University of Pisa
Pisa, Italy
{eleonora.marchetti, l.fanucci}@iet.unipi.it

A. Rocchi, M. De Marinis
Sensordynamics AG
Navacchio (PI), Italy
{aro,mdm}@sensordynamics.cc

***Abstract*—This paper presents an innovative and effective method to improve the performance of a micro mechanical gyroscope by introducing the damping of its sensing quality factor. Indeed the sensing quality factor is a key parameter for the micro mechanical gyroscope dynamic; particularly high sensing quality factor means long settling time, high response overshoot and high sensitivity to external disturbances (shocks and vibrations) that are typical of harsh automotive environment. For this reason micro mechanical gyroscopes employed in automotive environment need high shock and vibration immunity. This paper proposes a solution to reach this goal by adding a "virtual damping" to the system with an electrostatic feedback technique. This approach has been applied to a real automotive yaw gyro system, and simulations performed using Simulink™ environment show an appreciable output overshoot reduction, with the benefit of higher vibration immunity, once implemented the feedback technique.**

Micro mechanical gyroscope; electrostatic feedback technique; shock immunity enhancement

I. Introduction

Micro mechanical gyroscopes are key elements in several automotive systems like roll over detection and mitigation systems, navigation systems, Electronic Stability Program (ESP) and other systems for vehicle stabilizing and dynamic controlling [1]. Automotive systems are demanding gyroscopes characterized by high accuracy as well as high robustness and immunity against external perturbations (shocks and vibrations). In fact they have to provide an accurate output rate even in presence of environmental shocks and vibrations. One example is the roll over detection: some roll over events are triggered by impact with another object, such a curb, if the resulting shock saturates the gyro system, the airbag may not deploy. In a similar way, if a bump on the road causes a shock or a vibration which is translated into a rotational signal the airbag might deploy when it is not needed.

The vibration immunity can be enhanced by damping the sensing quality factor of the gyro. Indeed an electro mechanical gyro is composed by two coupled mechanical systems: a driving system and a sensing system. For the driving system a high quality factor is required in order to have high mechanical excitation with limited driving signals, on the contrary for the sensing system high quality factor involves long settling time, high response overshoot and high sensitivity to unwanted shocks and vibrations. This means that a key point to reduce the shock sensitivity is to control and reduce the gyroscope sensing quality factor.

In literature several quality factor control techniques have been proposed in the last year. For example, in laterally driven micro mechanical resonators [2] the quality factor is reduced by applying an electrostatic force between the planar resonant structure and the substrate in order to reduce the air damping gap. While in disk drive servo systems [3] an adaptive notch filter is usually used to suppress the mechanical resonance of the actuators.

The aim of this paper is to present an effective quality factor control strategy which can be applied to different gyroscope types (not only to laterally driven) and without exactly knowing the resonance frequency of the structure. The solution proposed is an electrostatic velocity feedback technique and performs the reduction of the quality factor by applying a "virtual damping" to the system.

The paper is organized as follows: section 2 describes the working principle of the feedback technique, section 3 shows the feedback implementation, section 4 presents the simulation results and the comparison with the state of the art and finally in section 5 conclusions are drawn.

II. Working Principle and Stability Issue

A vibratory gyroscope measures an angular rate and is based on the transfer of energy between two vibration modes caused by Coriolis acceleration. The operating principle of a single axis vibratory gyroscope is the following: the driving mass oscillates at resonance frequency around a driving axis (for example the z axis orthogonal to the xy plane), assuming that the sensing axis is the y axis, any angular rate about the x axis induces a Coriolis acceleration and in turn an oscillation of the sensing mass about the y axis. The applied angular rate (input rate) can be measured by processing the displacement signal in the direction of the sensing axis.

The sensing mass is a mechanical second order resonant system [4] and its transfer function in the Laplace domain is given by (1), where Ω_S is the displacement whose amplitude is proportional to the applied mechanical rate, and M_C is the Coriolis momentum.

978-3-9810801-5-5/DATE09 © 2009 EDAA

$$G(s)=\frac{\Omega_S(s)}{M_C(s)}=\frac{\gamma}{\left(s^2+s\dfrac{\omega_S}{Q_S}+\omega_S^2\right)}=\frac{\dfrac{1}{I}}{\left(s^2+s\dfrac{D}{I}+\dfrac{K}{I}\right)} \tag{1}$$

In (1) ω_S and Q_S are respectively the resonance frequency and the quality factor of the sensing system. The following definitions for ω_S and Q_S correlate the resonance frequency and the quality factor to the mechanical characteristics of the sensing system:

$$\omega_S=\sqrt{\frac{K}{I}}\ ,Q_S=\sqrt{K\cdot I}\cdot\frac{1}{D} \tag{2}$$

where K is the spring stiffness, I is the mechanical momentum of inertia and D is the damping factor.

From (2) is evident that the quality factor Q_S is inversely proportional to the damping factor D and can be reduced by adding a "virtual damping" (D_V) to the system. A virtual damping can be added with a derivator (K(s)) of gain equal to D_V used in a feedback structure to close the loop on the sensing system, as shown in Fig. 1.

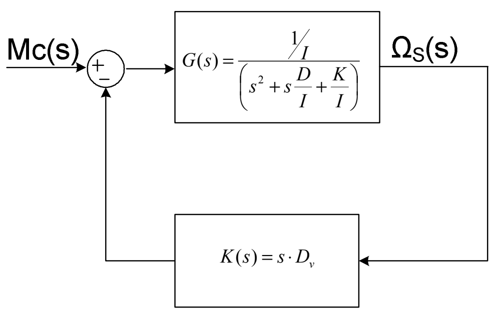

Figure 1. Working principle of the feedback loop

The transfer function of the closed loop is given by:

$$G_V(s)=\frac{\Omega_S(s)}{M_C(s)}=\frac{\gamma}{\left(s^2+s\dfrac{\omega_S}{Q_{SV}}+\omega_S^2\right)}=\frac{\dfrac{1}{I}}{\left(s^2+s\dfrac{D+D_V}{I}+\dfrac{K}{I}\right)} \tag{3}$$

$$Q_{SV}=\sqrt{K\cdot I}\cdot\frac{1}{(D+D_v)} \tag{4}$$

As expected the quality factor Q_{SV} of the closed loop system has been reduced by applying the velocity feedback and can be controlled trimming the gain D_V of the derivator block.

In the case of an ideal derivator the system is stable for any value of D_V and the quality factor can be damped without any limitation. Anyway a real derivator has at least one pole and the introduction into the system of one or more poles could lead to instability. For a derivator with three coincident poles the study of the root locus shows that there is a range of D_V values in which the system is stable but when D_V overcomes this range the system becomes instable.

The stability problem is a key issue in the design of the control loop, and the value of D_V has to be chosen properly to guarantee the system stability, as detailed in next sections.

III. FEEDBACK IMPLEMENTATION

A. *Possible feedback structures*

In a capacitive gyroscope the Coriolis momentum induces a mechanical displacement of the sensing mass that causes a variation in the capacitance of the sensing electrodes. The feedback chain described in the previous section adds to the Coriolis momentum a feedback momentum which damps the transient response due to the natural modes of the system. This feedback momentum is generated by applying a voltage to the gyro by means of dedicated capacitive electrodes.

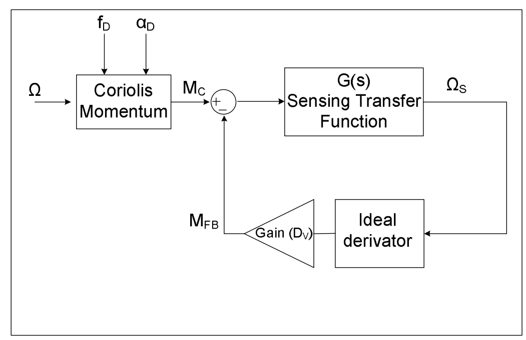

Figure 2. Pass band solution presented in [4]

In literature an electrostatic feedback technique based on the principle described above has been already presented [4] and Fig. 2 shows the solution adopted for its implementation. Since the input of the feedback chain is the sensor output, the loop must work in the frequency domain imposed by the gyroscope (pass band frequency domain). Consequently the loop works at high frequencies and this can be a drawback if the system employs digital blocks. In fact high frequency means high power consumption and thereby a base band solution is more desirable instead of a pass band solution.

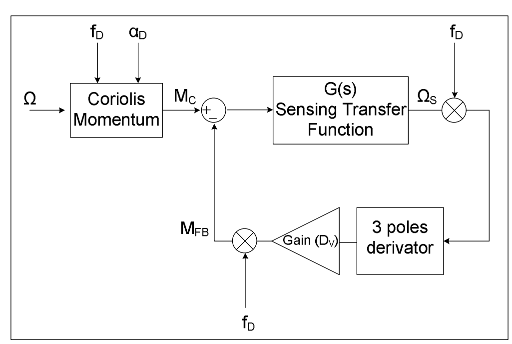

Figure 3. Base band proposed solution

This paper presents a base band approach for the implementation of the feedback technique. In fact in the proposed solution the feedback chain includes a demodulation stage (already used for the rate detection in the whole system) and a modulation stage (used to produce a feedback momentum which can be added to the Coriolis momentum) as shown in Fig. 3. Consequently the loop works in base band frequency domain. The use of a modulator and a demodulator stage does not involve a higher employment of electronic circuitry with respect to the previous solution. In fact the modulator stage can be implemented by the same digital block already used for rate demodulation in time sharing. Please note that this solution does not involve latency problems because the sampling frequency for the signal processing in the digital part of the system is much lower than the system clock. Both solutions have been implemented and simulated in Simulink™ environment to perform an objective comparison, but in following sections we focus on our base band proposal.

B. Simulink™ model of the base band feedback

The block diagram of the Simulink™ model developed for the base band feedback study is shown in Fig. 4.

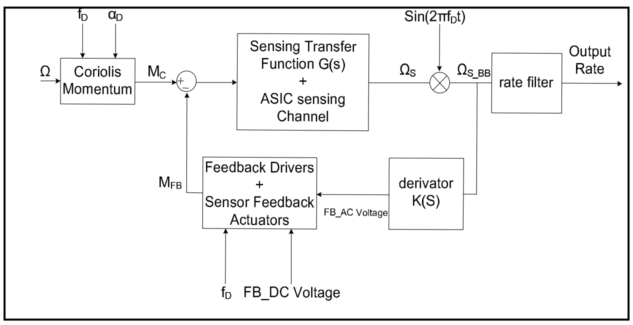

Figure 4. Block diagram of the Simulink™ model

The model consists of a vibratory gyroscope, a demodulation stage and a feedback loop. The input rate Ω together with the oscillation of the driving system produces a Coriolis momentum that causes the motion of the sensing mass. This motion is detected and elaborated to obtain the output rate. The block "Sensing Transfer Function+ASIC sensing channel" of Fig. 4 models both the gyro transfer function and the electronic needed to readout the capacitive sensing signal. While the Coriolis momentum (MC(t)) is modeled by implementing the well note expression:

$$M_C(t) = -2I\Omega(t) \times v_D(t) \tag{5}$$

where Ω(t) is the input rate and $v_D(t)$ is the angular velocity of the driving system that oscillates at the resonance frequency.

The demodulation stage is composed of the demodulator and a low pass filter (rate filter). And finally the feedback loop is composed of a three poles derivator (K(s)) of gain equal to D_V followed by a modulation stage and the electronic circuitry for the actuation of the feedback electrodes.

The feedback momentum responsible for the sensing quality factor damping arises from the application to the feedback electrodes of two opposite voltages (V_{FB_R} and V_{FB_L}) given by:

$$V_{FB\_R} = V_{FB\_DC} + V_{FB\_AC}\sin(2\pi f_D t) \tag{6}$$

$$V_{FB\_L} = V_{FB\_DC} - V_{FB\_AC}\sin(2\pi f_D t) \tag{7}$$

where f_D is the driving resonance frequency , V_{FB_DC} is the DC feedback voltage and V_{FB_AC} is the AC feedback voltage generated by the control loop.

The feedback momentum (M_{FB}) is the difference between the two electrostatic momenta generated by the voltages expressed in (6) and (7).

$$\begin{aligned} M_{FB} &= M_{FB\_R} - M_{FB\_L} = \frac{1}{2}(V_{FB\_R}^2 - V_{FB\_L}^2)\frac{dC_{FB}}{d\alpha_{FB}} \\ &= 2\frac{dC_{FB}}{d\alpha_{FB}}(V_{FB\_DC}V_{FB\_AC}\sin(\omega_D t)) = 2K_{fdbk}(V_{FB\_DC}V_{FB\_AC}\sin(\omega_D t)) \end{aligned} \tag{8}$$

Where C_{FB} and α_{FB} are respectively the capacitance and the rotation angle of the feedback electrodes.

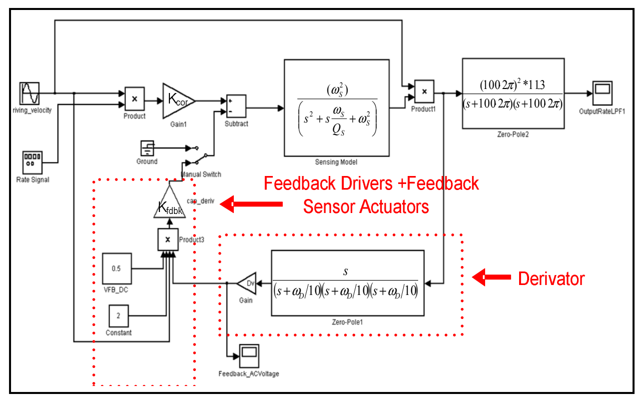

Figure 5. Simulink™ model of the feedback loop applied to a real yaw gyro readout system.

In the Simulink™ model the feedback momentum is implemented with the product expressed by (8) as shown in Fig. 5.

In order to have a model as close as possible to a real system the physical sensor parameters (2I and $dC_{FB}/d\alpha_{FB}$) have been extracted from laboratory measurements on a real automotive yaw gyro (developed by Sensordynamics AG) and are included in the parameter K_{Cor} and K_{fdbk} of the model.

An analytical study of the system has been performed in order to find an analytical expression for the amplitude A and the phase φ of the output rate. Assuming to have an input rate equal to $\Omega_i = \Omega\sin(\omega_\Omega t)$, the output rate is $\Omega_{S\_BB}(j\omega_\Omega) = A\sin(\omega_\Omega t + \varphi)$ where:

$$A = \frac{-\frac{|G(j\omega_{sum})|}{2}\cdot K_c \cdot \cos(< G(j\omega_{sum}) - \varphi)}{1 - \frac{|G(j\omega_{sum})|}{2} A_{loop}|K(j\omega_\Omega)|\cos(< G(j\omega_{sum}) + < K(j\omega_\Omega))} \tag{9}$$

$$\varphi = < G(j\omega_{sum}) - tg^{-1}\left(\frac{K2}{K_C}\right) \tag{10}$$

And:

$$K_C = I\Omega A_D \omega_D, \quad A_{loop} = \frac{K_{fdbk} V_{DC} D_V}{4}, \quad \omega_{sum} = \omega_D + \omega_\Omega$$

$$K1 = \frac{-\frac{|G(j\omega_{sum})|}{2} K_C}{1 - \frac{|G(j\omega_{sum})|}{2} A_{loop} |K(j\omega_\Omega)| \cos(< G(j\omega_{sum}) + < K(j\omega_\Omega))}$$

$$K2 = K1 \cdot A_{loop} |K(j\omega_\Omega)| \sin(< K(j\omega_\Omega) + < G(j\omega_{sum})) \tag{11}$$

Please note that in equations from (9) to (11), expressions $|K(j\omega)|$, $|G(j\omega)|$, $< K(j\omega)$ and $< G(j\omega)$ refer to the module and the phase of K and G transfer functions at a given frequency. The analytical expression of (9) has been plotted varying $f_\Omega = (\omega_\Omega / 2\pi)$ from 0 Hz to 2000 Hz and for different D_V values. The obtained results are shown in Fig. 6 and confirm the resonance damping.

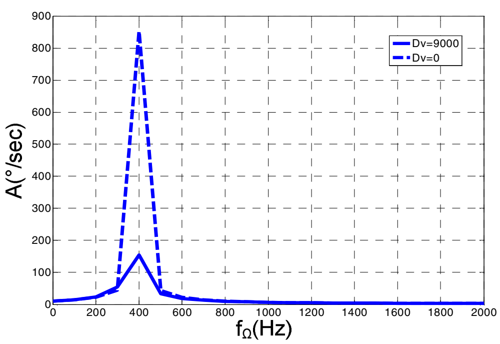

Figure 6. Output rate amplitude versus input rate frequency for feedback disabled (broken line), and feedback enabled (unbroken line)

As expected the resonance peak is lowered by the feedback loop. The peak of the frequency response is in correspondence of f_Ω=400 Hz because the simulations have been performed by assuming a resonance frequency for the driving system f_D=10 KHz, and a resonance frequency for the sensing system f_S=10.4 KHz. For Dv=0 the feedback is disabled and the resonance peak is around 850 °/sec, while for Dv=9000 the feedback is enabled and the resonance peak is lowered to 150°/sec. A Dv=9000 has been chosen because it is the maximum D_V value which guarantees the system stability.

C. *Enhanced base band feedback model*

Experimental measurements performed on the real yaw gyro used in the model show that the sensing resonance frequency depends on the feedback voltage. Particularly the variation of the resonance frequency (Δf_S) is given by:

$$\Delta f_S = -50\left(V_{FB\_DC}^2 + \frac{1}{2} V_{FB\_AC}^2\right) \tag{12}$$

In order to see how this phenomenon affects the feedback technique, an enhanced model has been developed in which the transfer function of the sensing system has been implemented to take into account the resonance variation. The transfer function G(s) of (1) can be elaborated as follows:

$$\Omega_S(s) \cdot \left(s^2 + s\frac{\omega_S}{Q} + \omega_S^2\right) = M_C(s) \cdot \gamma$$

$$\Omega_S(s) \cdot \left(1 + \frac{\omega_S}{Q_S}\frac{1}{s} + \omega_S^2 \cdot \frac{1}{s^2}\right) = M_C(s) \cdot \gamma \frac{1}{s^2}$$

$$\Omega_S(s) = M_C(s) \cdot \frac{\gamma}{s^2} - \Omega_S(s) \cdot \frac{\omega_S}{Q_S} \cdot \frac{1}{s} - \Omega_S(s) \cdot \frac{\omega_S^2}{s^2} \tag{13}$$

where γ depends on the momentum of inertia and isn't affected by the resonance variation. In our model γ has been set to the square value of the nominal resonance frequency. The block diagram of the resulting model is shown in Fig. 7.

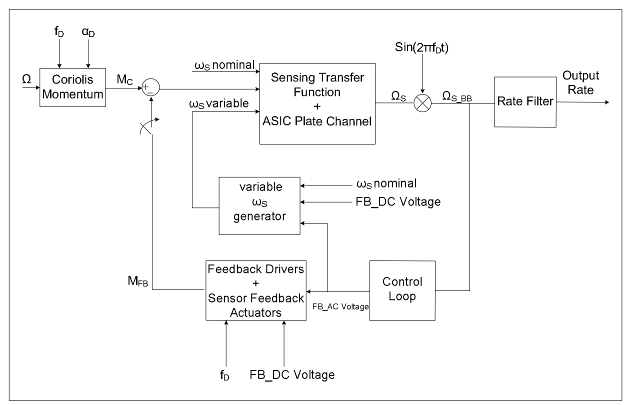

Figure 7. Block diagram of the enhanced base band feedback model

The gyro model is a Simulink block that implements the expression of (13) where ω_S is variable and is obtained by adding $\Delta\omega_S = 2\pi f_S$ to the nominal resonance frequency.

Simulation results show that the feedback loop keeps working properly as will be discussed in the next section.

IV. Simulation Results

In this section the results of the feedback models previously described are presented. More in details, section A shows the simulation results related to the base band feedback implementation, section B presents the simulation results related to the enhanced base band model and finally section C compares the pass band and the base band feedback implementation.

A. Simulation results of the feedback base band model

The feedback model has been simulated with the following setup:

- gyro parameters: Q_S=1000, f_D=10 KHz, f_S=10400 Hz;
- experimental coefficients: K_{Cor}=3.419, K_{fdbk}=1.284x10^3;
- input rate Ω: square wave (Amplitude=100°/sec and frequency =6.1 Hz);
- rate filter: second order low pass filter (cut frequency equal to 100 Hz);
- feedback chain: D_V=9000 (maximum value to keep the system stable).

The following figure shows the output rate resulting from the simulation when the feedback chain is enabled with a delay of 0.2 sec.

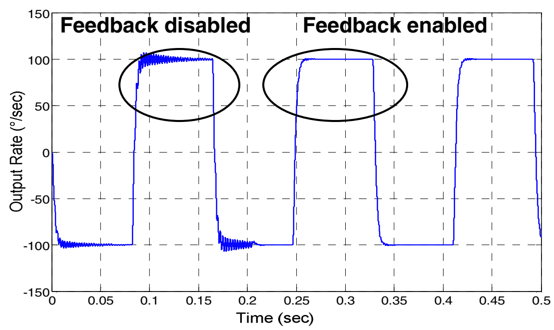

Figure 8. Output rate with the feedback enabled after 0.2 sec

As long as the feedback is disabled there is a residual oscillation, due to the 400 Hz component of the input square wave, which is completely suppressed when the loop is enabled. The residual oscillation could be suppressed by using a more selective low pass filter but this approach entails two drawbacks: limits the system bandwidth and doesn't suppress the oscillation inside the sensing system.

As said above a limitation on the D_V value is the system stability, another limitation is the maximum feedback voltage. In fact when the amplitude of the input square wave (Ω) increases the feedback voltage needed to perform the damping arises too. Assuming that the maximum feedback voltage is 0,5V (saturation limit) and keeping D_V equal to the maximum value for the stability of the system, the maximum amplitude of the input square wave is around 200°/sec. This value has been extracted by including a saturator block in the model and varying Ω between 0 and 1000°/sec (Fig. 9) with a step of 100°/sec.

When the amplitude of the input rate reaches 200°/sec the feedback voltage saturates at 0,5V and we expect worse oscillation suppression. The overshoot on the output rate has been calculated varying Ω from 0 to 1000°/sec with step of 100°/sec. Simulation results show that the saturation of the feedback voltage does not appreciably affect the output overshoot (Fig. 10).

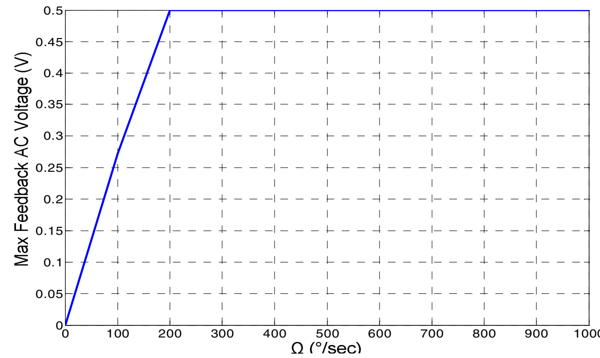

Figure 9. Maximum feedback voltage versus input rate amplitude

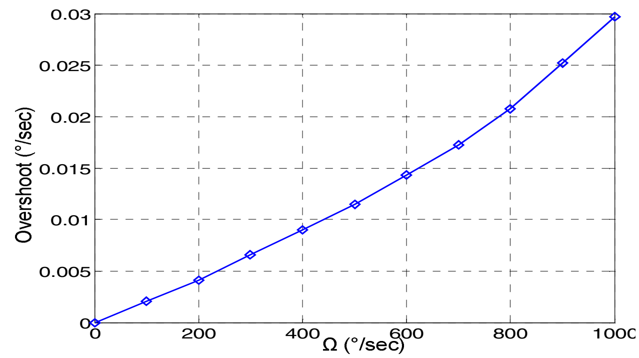

Figure 10. Overshoot on the output rate versus Ω variation

When Ω exceeds 200°/sec the slope of the overshoot curve slightly increases as expected but this does not significantly change the effectiveness of the feedback loop. The advantages due to the introduction of the feedback loop are evident from the overshoot analysis in the two cases of feedback disabled and feedback enabled. Fig. 11 shows that the feedback for the resonance damping significantly reduces the output overshoot with the benefit of higher vibration immunity.

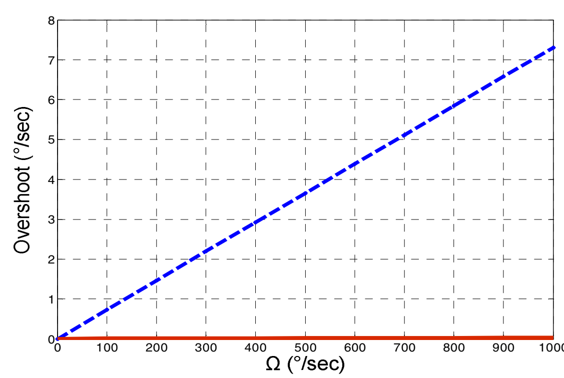

Figure 11. Overshoot with (unbroken red line) and without (broken blue line) feedback loop

The overshoot without feedback can not be well visualized because it varies only from 0°/sec to 0.03°/sec.

B. Simulation results of the enhanced base band feedback model

The system still works properly when taking into account the variation of the resonance frequency due to the feedback voltage. In fact simulation results show that the overshoot resulting from the enhanced model is even lower than the overshoot resulting from the simple model (Fig. 12).

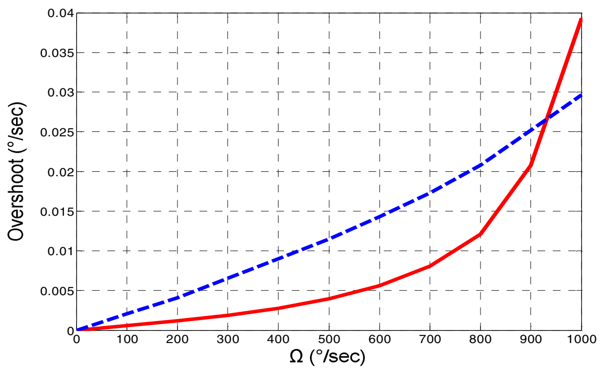

Figure 12. Output overshoot for base band model (broken blue line) and for enhanced base band model (unbroken red line)

C. Comparison between the base band and the pass band model

The pass band feedback technique has been modeled and simulated too. The analysis of the obtained results shows that the pass band implementation has a lower efficiency, in fact a higher feedback voltage is needed to perform the resonance damping. Consequently the saturation of the feedback voltage occurs for lower value of the input rate amplitude. In fact the feedback saturation voltage is in correspondence of an input rate of 120°/sec instead of 200°/sec (Fig. 13).

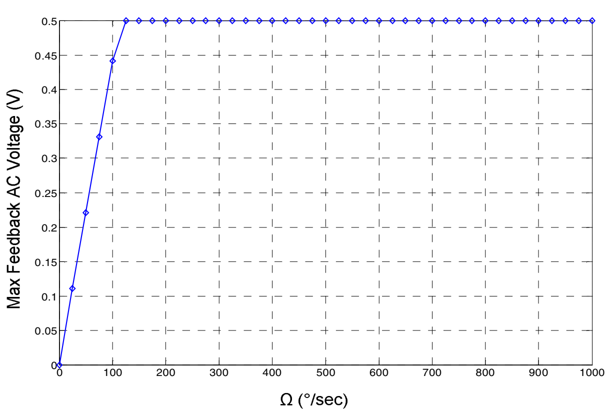

Figure 13. Maximum feedback voltage versus amplitude for pass band implementation

V. CONCLUSIONS

An innovative approach to enhance shock immunity in automotive yaw gyro has been presented. The solution proposed is based on the damping of the gyro sensing resonance by means of a base band feedback loop technique. This technique has been studied and simulated in Simulink™ environment by using the model of a real automotive yaw gyro system and has been compared with a pass band feedback technique already presented in literature. From the analysis of the results the following conclusions can be drawn. Firstly, the proposed feedback technique involves an effective reduction of the overshoot on the output rate also taking into account real system limitations such as the maximum feedback voltage and the system stability. Secondly the proposed base band solution results more effective than the pass band solution presented in literature. And finally the effectiveness of the feedback loop does not change taking into account secondary effects such as the variation of the resonance frequency due to the application of the feedback voltage. These points make the proposed approach the ideal candidate for shock-immune gyro system that will be then produced as follow-up of this study.

REFERENCES

[1] R. Neul et all, “Micromachined Gyros for Automotive Applications”, Sensors 2005 IEEE, pp. 527–530, 30 Oct-3 Nov 2005.

[2] K. B. Lee, Y.-H. Cho, “An electrostatic quality factor control for surface-micromachined lateral resonators”, Proc. of the Seventh International Symposium on Micro Machine and Human Science , pp. 143-147, 2-4 Oct. 1996;

[3] C.-I. Kang, C.-H. Kim, “An adaptive notch filter for suppressing mechanical resonance in high track density disk drives”, Microsyst. Technol., vol. 11, pp. 638-652, 2005;

[4] C. Jeong, S. Seok, B. Lee, H. Kim and K. Chun, “A study on resonant frequency and Q factor tunings for MEMS vibratory gyroscopes”, J. Micromech. Microeng., vol. 14, pp. 1530-1536, 2004.